47th AIAA/ASME/ASCE/AHS/ASC Structures, Structural Dynamics and Materials Conference, May 1-4, 2006 Newport, Rhode Island

Comparative Analysis of Computational Methods for Limit-Cycle Oscillations

Arathi K. Gopinath*,
Stanford University, Stanford, CA 94305-4035
Philip S. Beran†
Air Force Research Laboratory, Wright-Patterson AFB, OH 45433
and
Antony Jameson‡
Stanford University, Stanford, CA 94305-4035

Various methods are explored in the computation of time-periodic solutions for autonomous systems. The purpose of the work is to illuminate the capabilities and limitations of methods, including a new method developed as part of the work, not based on time integration, for the fast computation of limit-cycle oscillations (LCO). Discussion will focus on methodology, robustness, accuracy, and frequency prediction. Results for two simplified model problems are presented in which temporal discretization errors during LCO are taken to machine zero. One, a typical airfoil section with nonlinear structural coupling and the other, a nonlinear panel in high speed flow. Treatment of sharp transients during LCO is also discussed.

I. INTRODUCTION

Limit-cycle oscillation (LCO) is a limited-amplitude, self-sustaining oscillation produced by an aero-structural interaction. LCO results in an undesirable airframe vibration and limits the performance of the flight vehicle.

The prediction and alleviation of LCOs in air vehicles continues to be a challenge. State-of-the-art computational techniques for predicting LCO responses in aeroelastic systems still use time-integration methods which require a great deal of computational effort which translates into long turn-around times. When LCOs experience a limited number of periods of sharp response, the number of variables needed to discretize the cycle can be quite large. It becomes crucial to keep the expansions compact especially for systems with many spatial variables.

These features make these methods not suitable for design optimization or routine use in the test and evaluation environment. The goal of the current work is to determine the range of applicability of models of varying fidelity to the numerical prediction of LCOs and the development of fast spectral methods for evaluating the dependence of LCOs on stochastic system parameters.

*Doctoral Candidate, AIAA Student Member.

†Principal Research Aerospace Engineer, Multidisciplinary Technologies Center, Air Vehicles Directorate,AIAA Associate Fellow

‡Thomas V. Jones Professor of Engineering, Department of Aeronautics and Astronautics, AIAA Member

A cyclic method was developed to compute LCOs for potentially large, nonlinear, multidisciplinary systems of equations.[1] To improve on this 2nd-order cyclic/finite difference method, two spectral based techniques are implemented. One is the time spectral method[2] developed at Stanford University which is along the lines of the harmonic balance method[3] developed at Duke University. These are algorithms that use a Fourier representation in time. The second method is the spectral element method[4,5] implemented here in a novel way for periodic systems in time. A space-time finite element method has been used previously[6,7] for predicting the periodic steady-state in helicopter rotor dynamics using an aeroelastic analysis.

This paper will compares and contrasts the three methodologies, their robustness, accuracy and frequency prediction capabilities. A simple model of an aeroelastic airfoil with nonlinear structural coupling is used to demonstrate the efficacy of the procedure in detail. In addition, results for a nonlinear semi-infinite panel problem is discussed.

II. Formulation

In this section, the mathematical formulation of the problem is described. The cyclic method in combination with the finite difference method for the time discretization has been described in previous work.[1] The cyclic method is described here for clarity. Two other computational techniques, the Time Spectral method and the Spectral Element method is used in conjunction with the cyclic method in place of the finite difference discretization.

A. Cyclic Method

Time-periodic solutions of the autonomous system

$$\frac{d\mathbf{x}}{dt} = \mathbf{f}(\mathbf{x}, \lambda)$$

are sought, where t is time, $\mathbf{x}(t)$ is an N_f-dimensional array of real variables, and f is an array of N_f nonlinear functions, dependent on $\mathbf{x}$ and a free parameter λ. The period of the response is denoted by T, such that

$$\mathbf{x}(t) = \mathbf{x}(t+T).$$

The time variable is scaled, $s \equiv t/T$, leading to an equation in which the period appears explicitly,

$$\frac{d\mathbf{x}}{ds} = T\mathbf{f}(\mathbf{x}, \lambda). \tag{1}$$

A set of points on the periodic orbit at N_t time levels is selected, leading to an expanded set of $N_t N_f$ unknowns,

$$\mathbf{X} \equiv (\mathbf{X}_1, \mathbf{X}_2, ...\mathbf{X}_{N_t})^T = (\mathbf{x}(s_1), \mathbf{x}(s_2), ..., \mathbf{x}(s_{N_t}))^T,$$

where the subscript specifies the time level(i.e., $s_{j+1} = s_j + \Delta_s$; $\Delta_s = 1/N_t$ when N_t are uniformly distributed).

Using the trapezoidal rule, (1) is discretized to yield an expanded collection of equations:

$$\mathbf{G}_j \equiv \frac{T}{2}(\mathbf{F}_{j-1} + \mathbf{F}_j) - \left(\frac{d\mathbf{X}}{ds}\right)_j = 0 \qquad (j = 1, ..., N_t), \tag{2}$$

where $\mathbf{F}_j \equiv \mathbf{f}(x(s_j))$. The time derivative term $\frac{d\mathbf{X}}{ds}$ is discretized using three different strategies and is described in later sections.

A closed set of equations,

$$\mathbf{G} \equiv (\mathbf{G}_1, \mathbf{G}_2, ..., \mathbf{G}_{N_t}, \mathbf{G}_{N_t+1}, \mathbf{G}_{N_t+2})^T = 0,$$

is obtained by adding a pair of scalar constraints to (2) that prevent the solution from being trivial (i.e. $\mathbf{X} = 0$ for all j):

$$\mathbf{G}_{N_t+1} \equiv (\mathbf{X}_j)_{k_1} - \beta_1 = 0, \tag{3}$$

$$\mathbf{G}_{N_t+2} \equiv (\mathbf{X}_j)_{k_2} - \beta_2 = 0, \tag{4}$$

where j is an arbitrary point on the cycle, usually taken to be 1, and k_1 and k_2 are indices corresponding to two different variables at that time instance. Constraint (3) is used to identify the "starting" point of the cycle, such that $\beta_1 = 0$ (assuming an oscillation approximately centered about 0 for the selected variable). Likewise, (4) is used to set the amplitude of the cycle, such that $\beta_2 \neq 0$.

The addition of two equations is accompanied by an increase in the number of unknowns by 2. These unknowns are $\mathbf{X}_{N_t+1} \equiv \lambda$ and $\mathbf{X}_{N_t+2} \equiv T$. Thus, a total of $N_t N_f + 2$ equations are solved for not only the LCO solution, but also the period of the oscillation and the value of the free parameter λ at which the LCO meets the amplitude constraint (4).

In symbolic form, the complete system of "cyclic" equations is expressed as

$$\mathbf{G}(\mathbf{X}) = 0, \tag{5}$$

where this system is solved for expanded form of $\mathbf{X}$,

$$\mathbf{X} = (\mathbf{X}_1, \mathbf{X}_2, ...\mathbf{X}_{N_t}, \lambda, T)^T.$$

System (5) is solved with Newton's method, and IMSL/LAPACK routines are used to carry out the matrix calculations.

B. Constructing the Time Derivative Operator

In the next few subsections the three different methodologies used to construct the time derivative term, $D_s\mathbf{X}$ is discussed. This is used in combination with (2) in the cyclic formulation explained earlier. One is the finite difference method which has been discussed previously by Beran et.al. [1] Second is the Time Spectral method which uses global basis functions. And the last one is the Spectral Element method which divides the orbit into number of sub-time intervals and represents each interval with a polynomial of order P.

1. Finite Difference Formulation

The time derivative term is discretized using finite differences, so that,

$$(D_s\mathbf{X})_j \equiv \left(\frac{d\mathbf{X}}{ds}\right)_j = \frac{\mathbf{X}_{j+1} - \mathbf{X}_j}{\Delta_s}.$$

Periodicity is enforced in closing (5) at the end points. For the form of discretization described above, the last equation takes the form,

$$(D_s\mathbf{X})_{N_t} \equiv \left(\frac{d\mathbf{X}}{ds}\right)_{N_t} = \frac{\mathbf{X}_1 - \mathbf{X}_{N_t}}{\Delta_s}.$$

With this modification, the time derivative operator takes the shape of a periodic-banded structure, i.e. a banded matrix with a wrap-around term.

2. The Time Spectral Method

The Time Spectral Method was originally proposed and validated in.[2] This method falls into the same category of algorithms called Harmonic Balance methods developed by K. Hall[3] from Duke University and Nonlinear Frequency Domain methods developed by McMullen et.al.[8,9] from Stanford University. This class of algorithms take advantage of the periodic nature of the problem, and use a Fourier representation in time. Whereas Harmonic Balance techniques use Fast Fourier Transforms (FFTs), the Time Spectral method works in the time domain by expressing the time-derivative operator as a matrix operator.

Recall that

$$\mathbf{X} = (\mathbf{X}_1, \mathbf{X}_2, ...\mathbf{X}_{N_t}, \lambda, T)^T$$

where

$$\mathbf{X}_1 = (x_1, x_2, x_3, ..., x_{N_f})_1,$$

i.e., $\mathbf{X}_1$ is an array of all points in the N_f-dimensional array at time level 1. Construct an array $\mathbf{w}$ which consists of one variable at all time levels. The discrete Fourier transform of $\mathbf{w}$, for a time period "1" (scaled time s has a period of 1), is given by

$$\hat{w}_k = \frac{1}{N_t} \sum_{n=0}^{N_t-1} w^n e^{-ik2\pi n\Delta_s}$$

and its inverse transform,

$$w^n = \sum_{k=-\frac{N_t}{2}}^{\frac{N_t}{2}-1} \hat{w}_k e^{ikn2\pi\Delta_s}, \tag{6}$$

where the time period is divided into N_t equal time intervals(N_t even), $\Delta_s = 1/N_t$.

From (6), the time discretization operator D_s can be written as

$$D_s w^n = 2\pi \sum_{k=-\frac{N_t}{2}}^{\frac{N_t}{2}-1} ik\hat{w}_k e^{ik2\pi n\Delta_s}.$$

This summation involving the Fourier modes $\hat{w}_k$, can be rewritten in terms of w in the time domain, both for even and odd N_t as,[2,10,11]

$$D_s^{even} w^n = \sum_{m=-\frac{N_t}{2}+1}^{\frac{N_t}{2}-1} d_m^{even} w^{n+m},$$

and

$$D_s^{odd} w^n = \sum_{m=\frac{1-N_t}{2}}^{\frac{N_t-1}{2}} d_m^{odd} w^{n+m},$$

where

$$d_m^{even} = \begin{cases} \pi(-1)^{m+1} \cot(\frac{\pi m}{N_t}) & : \quad m \neq 0 \\ 0 & : \quad m = 0 \end{cases}$$

and

$$d_m^{odd} = \begin{cases} \pi(-1)^{m+1} cosec(\frac{\pi m}{N_t}) & : \quad m \neq 0 \\ 0 & : \quad m = 0 \end{cases}$$

Note that $d_{-m} = -d_m$ for both even and odd N_t. Hence D_s takes the form of a central difference operator connecting all the time levels, yielding an integrated space-time formulation which requires the simultaneous solution of the equations for all time levels.

Since the computation of D_s involves terms at all the time levels (i.e., full stencil), the time derivative matrix operator is full, which is typical of spectral methods. And since spectral methods use global basis functions in the form of sines and cosines, periodicity need not be explicitly enforced.

3. Spectral Element Formulation

The spectral element method is a high-order finite element technique pioneered by Patera.[4] As the name suggests it combines the geometric flexibility of finite elements with the high accuracy of spectral methods. Spectral methods are essentially discretization methods for the solution of partial differential equations expressed in a weak form. It is assumed that the solution can be expressed as a series of polynomial basis functions, which can approximate the solution well in some norm, as the polynomial degree tends to infinity. Typically the basis is chosen to be orthogonal in a weighted inner-product. Lagrange interpolants are used within each element, where the nodes of these shape functions are placed at the zeros of Legendre polynomials(Gauss-Lobatto points).

In this section, the formulation of the spectral element method for the system (1) will be presented. First, multiply (1) by the test function $v(s)$ and integrate over the orbit to get the weak form of the equation,

$$\oint v(s)\frac{dw}{ds}ds = \oint v(s)Tf(w(s))ds.$$

Using periodicity and the chain rule, rewrite as,

$$-\oint w(s)\frac{dv}{ds}ds = T\oint v(s)f(w(s))ds.$$

Since the entire orbit/domain is divided into a number of sub-time intervals, consider the integral in each interval,

$$-\int_{\Omega_j} w_j(s)\frac{dv_j}{ds}ds = T\int_{\Omega_j} v_j(s)f_j(w(s_j))ds,$$

using $v_j(s) = \phi_j$

$$T\int_{\Omega_j} \phi_j^p f_j(w(s_j))ds + \int_{\Omega_j} w_j(s)\frac{d\phi_j^p}{ds}ds = 0.$$

Using a change of variables, $s = s_j + \frac{\psi+1}{2}(s_{j+1} - s_j)$, rewrite as

$$T\int_{-1}^{1} \phi_j^p(\psi)f_j(w(\psi))\frac{ds}{d\psi}d\psi + \int_{-1}^{1} w_j(\psi)\frac{d\phi_j^p}{d\psi}d\psi = 0$$

This equation is integrated using Gauss quadrature within each sub-time interval. Since the orbit is divided into sub-intervals, the time derivative in each sub-interval is directly dependent only on the points in its own sub-interval. In this way, some level of sparsity is retained, at the same time, high accuracy is ensured by using high-order polynomials within each sub-interval. Periodicity is enforced during global assembly by wrapping around the first and last elements.

Three different extension procedures are discussed for the test problems. *h*-extension refers to the procedure when fixed low-order polynomials are used on successively finer meshes/elements (increasing number of sub-time intervals). This typically produces algebraic convergence of the order of the polynomial degree.

P-extension procedure converges exponentially for smooth solutions and these are obtained when the number of sub-time intervals are held fixed while increasing the order of the polynomial. hP-extension combines both these strategies and has the potential to produce exponential convergence even for non-smooth problems. It achieves this by increasing the polynomial order while changing/refining the mesh/spacing between the intervals.

III. Current Results

A. The Airfoil Problem

The aeroelastic system studied here is a nonlinear symmetric airfoil in low-speed flow, described by two physical DOFs: pitch and plunge. The plunge DOF has linear stiffness but the pitch DOF includes a third-order and fifth-order stiffness terms in addition to the linear component. Hence, the restoring force associated with the torsional spring is expressed as $K_\alpha(\alpha + k_3\alpha^3 + k_5\alpha^5)$, where K_α is the dimensional linear stiffness and k_3 and k_5 are the dimensionless parameters governing the third- and fifth- order nonlinearities respectively. The free parameter λ, is defined to be a nondimensional parameter proportional to flight speed ("reduced velocity"), which when sufficiently large, leads to flutter or LCO responses of the system. The airfoil dynamics are represented by a system of eight ODEs, obtained through linear modeling of the aerodynamics.[12] The final form of the 8-DOF system is given in .[13] The details of the Hopf bifurcation can be found in.[1] A typical LCO branch is shown in Figure 1.

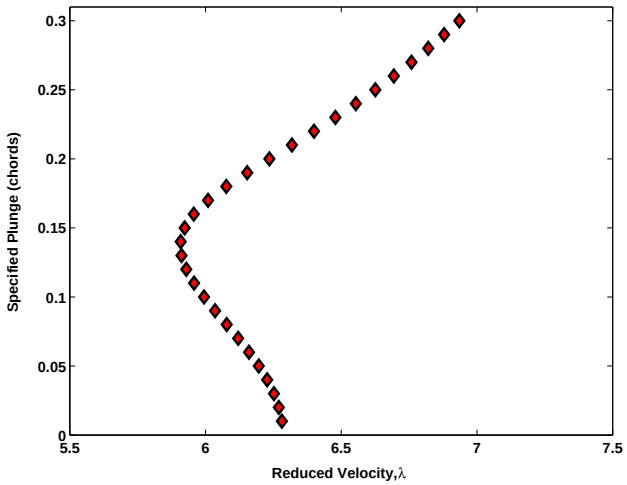

Figure 1. An LCO branch showing sub-critical Hopf bifurcation

The computation of cyclic solutions requires the specification of initial conditions for the iterative process. Time integrations of system response in pitch and plunge revealed a clock-wise rotation of the phase portrait in these two parameters (pitch plotted on the abscissa). An initial approximation to the LCO dynamics was imposed by assuming a circular trajectory in pitch and plunge, using the target cross-over value of plunge (β_2) to set the LCO amplitude.

The parameters governing the LCO (Equations 3 and 4) are a specified plunge value (β_2) at a vanishing angle of attack (β_1). Plunge values are reported in non-dimensional form, using airfoil chord as a scale factor. The torsional spring parameters k_3 and k_5 are specified to be -3 and 20 respectively, to produce a sub-critical Hopf bifurcation.[14]

Figure 2 (a) and (b) show comparisons of LCO branches in terms of specified values of β_2 for selected number of scaled time intervals per cycle (N_t) using finite difference method and time spectral method respectively. Note that as β_2 decreases, the LCO response weakens. The selection of N_t=100 leads to LCOs well converged in time step over most of the range in β_2 for the finite difference case. Whereas the time spectral method captures the LCO branch over the entire range of β_2 with just 40 scaled time intervals, to plotting accuracy.

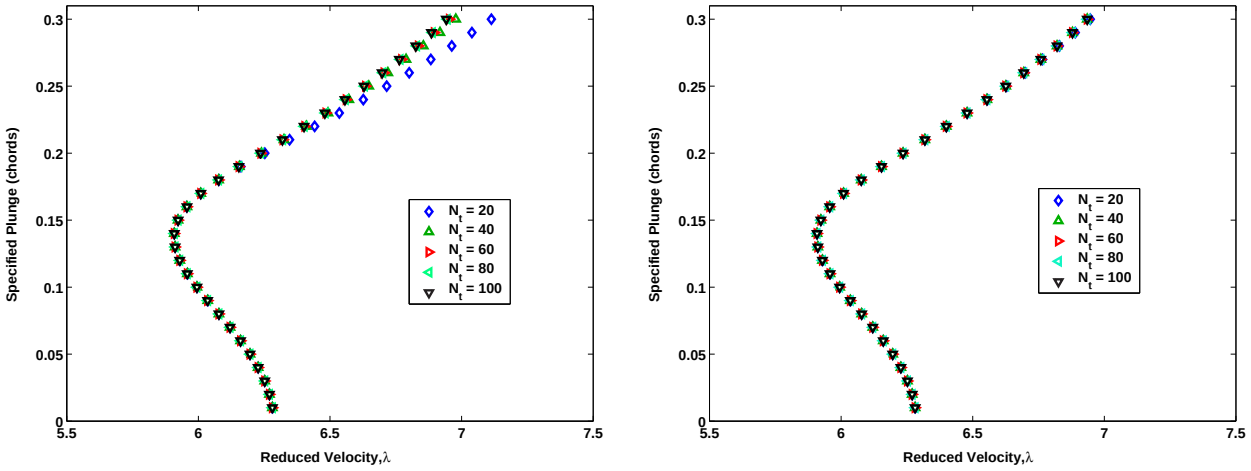

(a) Finite Difference (b) Time Spectral method

Figure 2. Comparison of LCO branches in terms of specified β_2 for selected numbers of scaled time steps per cycle (N_t) using Finite Difference and Time Spectral methods

A strong nonlinear response is observed beyond the subcritical Hopf bifurcation point computed at about $\lambda = 6.29$. This is further illustrated in Figures 3 and 4. Figure 3 (a) shows the LCO (pitch vs. plunge), (b) shows the initial and final solution of variation of pitch as a function of scaled time and (c) the initial and final solution of plunge, computed at $\beta_2 = 0.3$ and $\lambda = 6.9351$.

Similarly, the phase-plane plots for $\beta_2 = 0.15$, a point close to the cyclic fold, are shown in Figure 4. This point shows a weaker response and hence requires fewer time intervals for high accuracy. The pitch and plunge also show a "sine"-like behavior which can be captured with fewer frequencies. Whereas for the strong nonlinear response point, the pitch curve shows a marked asymmetry and a variation unlike a "sine" function. These also transform into sharp-transients in the LCO plots, moving away from the "ellipse"-like structure. These characteristics require larger number of time intervals or DOF to be captured to high levels of accuracy. Spectral based techniques with their high-order polynomial formulation have the ability to capture these features with fewer DOFs.

Figure 5 shows the log-log ($T - T_c$) error plot with refinement in N_t computed with the 3 different computational techniques for the strong nonlinear response point, $\beta_2 = 0.3$. Here T_c is the time period computed with 200 time intervals per cycle with the time spectral method. The convergence of the cyclic/FD method is verified to be second-order (algebraic convergence). Convergence of the cyclic/time spectral method using odd number of N_t shows near exponential convergence. This algorithm shows machine precision accuracy with just 70 DOFs. Cyclic/spectral element h-extension (increasing h, keeping P fixed, P=2) also shows algebraic convergence. A P-extension (increasing P, keeping h fixed, $N_t = 2$), shows close to exponential convergence.

Similarly, Figure 6 shows the log-log error plot for a weaker LCO point, $\beta_2 = 0.15$. Convergence rates are very similar to the strong response point, but the cyclic/time spectral method converges to machine precision using only 40 DOFs. As explained earlier, this is attributable to the fact that the frequency content for this

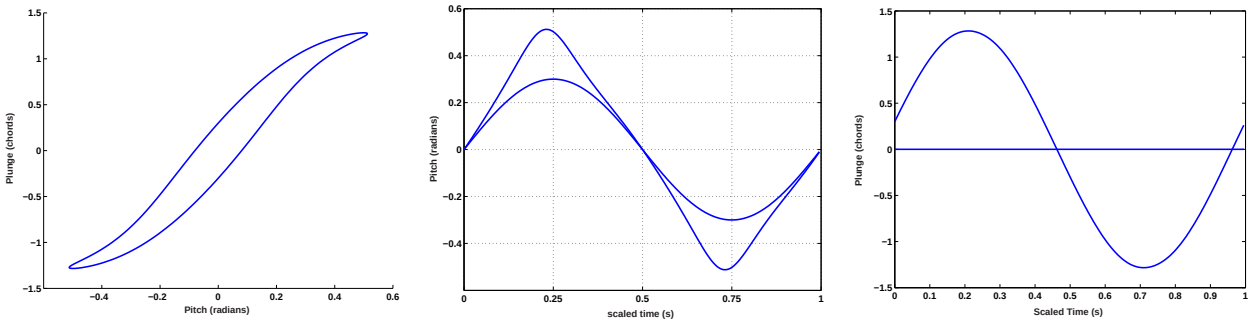

(a) LCOs (b) Time history of pitch (c) Time history of plunge

Figure 3. Phase-plane plots computed for $\beta_2 = 0.3$ (initial and final iterate of pitch and plunge shown)

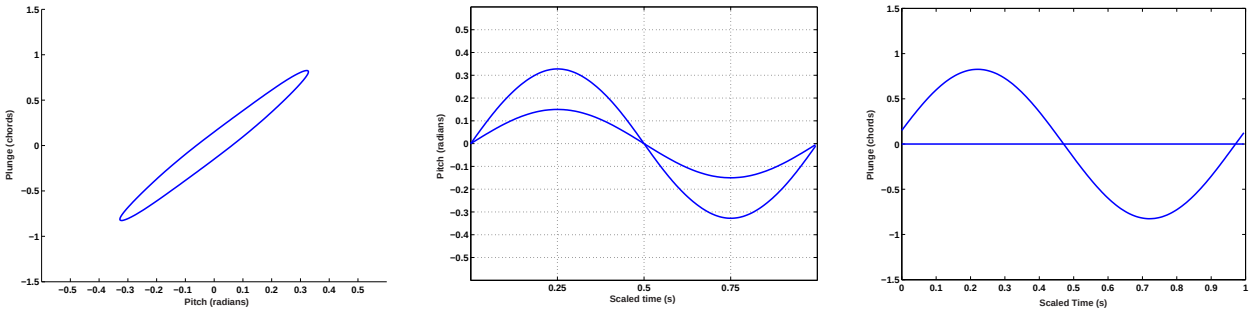

(a) LCOs (b) Time history of pitch (c) Time history of plunge

Figure 4. Phase-plane plots computed for $\beta_2 = 0.15$ (initial and final iterate of pitch and plunge shown)

case is lower, as shown in Figure 4. Also, for small number of DOF ($N_t < 10$), this case shows smaller error compared to the $\beta_2 = 0.3$ case.

1. Adaptive Cyclic/Spectral Elements and hP-extension

It was shown in the previous section that in regions of strong nonlinear response, high-order schemes are required to achieve good levels of accuracy. For instance, in the airfoil case, it was shown that for $\beta_2 = 0.3$, there were regions of rapid-transients which required higher resolution to be captured compared to other regions in the orbit. This is clearly seen in Figure 3 (a). In the Spectral Element method, with h-extension, one would increase h uniformly, keeping P the same. When h is increased, resolution is increased everywhere in the orbit, even in regions which are already well resolved. In the P-extension procedure, the polynomial order is uniformly increased fixing h. Again the order of the polynomial is increased even in regions which are well resolved. Both these methods could be prohibitive for large systems with isolated regions of sharp transients. In this section, we investigate a case where the Cyclic/Spectral Element is modified to adaptively refine only in regions of sharp-transients.

We again consider the airfoil problem at a strong nonlinear response point, $\beta_2 = 0.3$ and divide its orbit into 6 sub-time intervals. A polynomial of order P is chosen in each interval. We observe the convergence of the error in computed time period T as P is uniformly increased. h is held fixed at 6 but the spacing between the intervals will be allowed to change, thus refining in regions of high-transients. Figure 7 (b) shows the time history of the converged pitch. The blue circles show equal spaced intervals. (Note the marked asymmetry

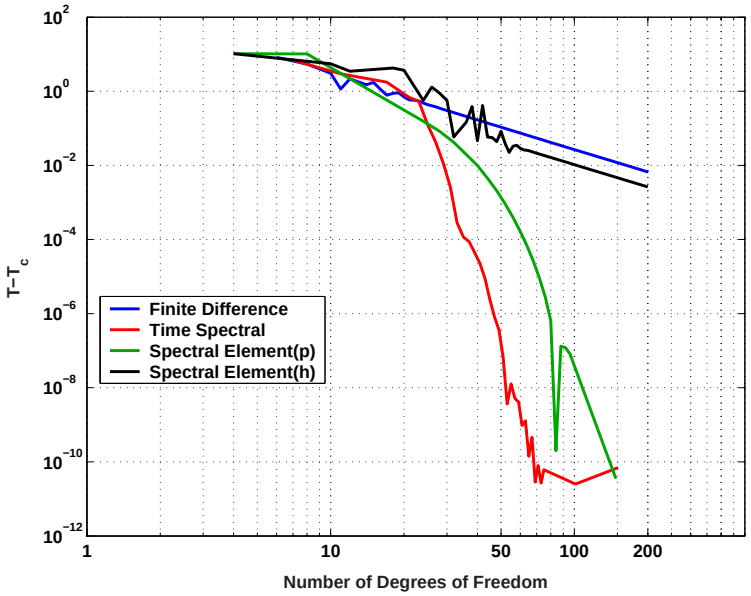

Figure 5. Error in computed time period using the three different computational methods for $\beta_2 = 0.3$

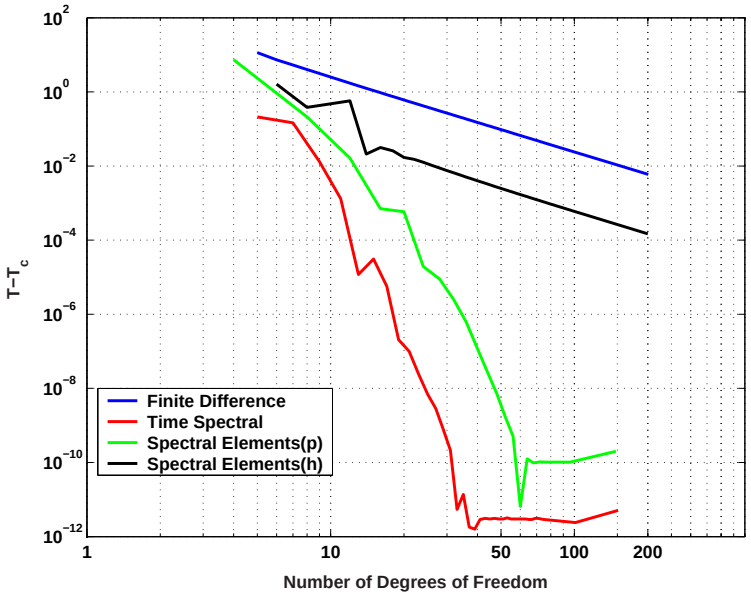

Figure 6. Error in computed time period using the three different computational methods for $\beta_2 = 0.15$

of the pitch curve producing the sharp-transients as mentioned earlier.) The red curve in Figure 7 (a) shows the convergence with equal spacing throughout (P-extension), while the blue curve shows the convergence as the intervals are uniformly refined in regions of high "activity"(hP-extension). The adaptive Cyclic/Spectral Element method also converges with far fewer DOF. In regions marked B, the difference between the two approaches could be as much as two orders of magnitude. Hence with adaptive Cyclic/Spectral Elements, we achieved even better convergence than what we achieved with the P-extension procedure earlier.

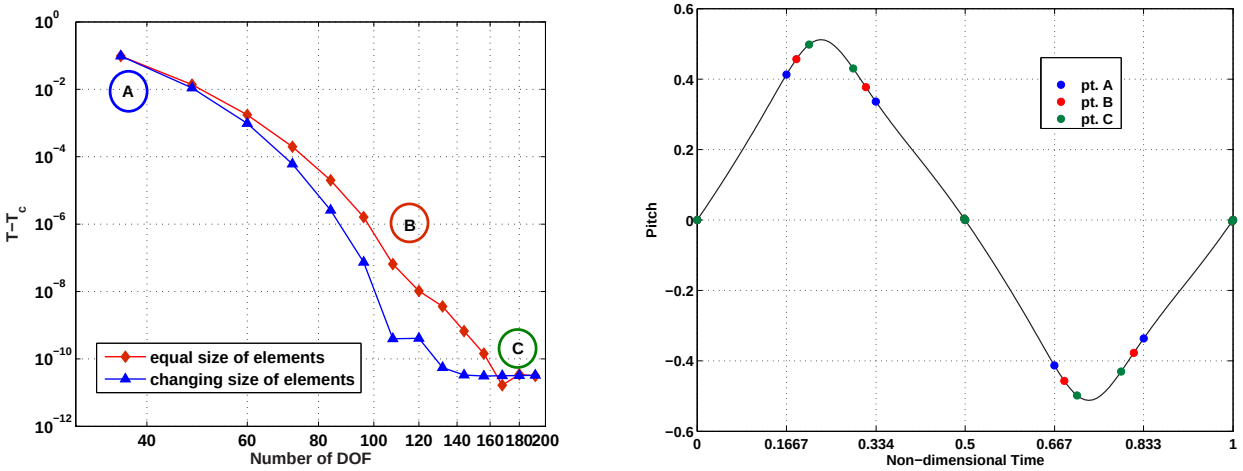

(a) Plot of error in time period

(b) Pitch as function of time

Figure 7. Comparison between Cyclic/SE and adaptive Cyclic/SE for the Airfoil Problem at $\beta_2 = 0.3$

B. The Panel Problem

High speed flow over a semi-infinite, pinned panel is considered. Panel dynamics are computed with the nondimensional form of von Karman's large-deflection plate equation. The local, instantaneous panel deflection, is denoted by $w(x,t)$ and is nondimensionalized by h, the panel thickness. Two pinned boundary conditions are enforced at the panel's endpoints: $w = 0$ and $\frac{\partial^2 w}{\partial x^2} = 0$. The airloads are modeled with first-order piston theory allowing these loads to be related to local plate slope and velocity. The governing equation reduces to:

$$\frac{\mu}{\lambda}\frac{\partial^4 w}{\partial x^4} - \hat{N}\frac{\partial^2 w}{\partial x^2} + \frac{\partial v}{\partial t} = -\frac{\mu}{\sqrt{M_\infty^2 - 1}}\left[\frac{\partial w}{\partial x} + \left(\frac{M_\infty^2 - 2}{M_\infty^2 - 1}\right)v\right], \tag{7}$$

$$\hat{N} \equiv \frac{6\mu}{\lambda}\left(\frac{h}{L}\right)^{-2}(1-\nu^2)\int_0^1 \left(\frac{\partial w}{\partial x}\right)^2 dx.$$

Panel velocity $v = \frac{\partial w}{\partial t}$ has been introduced. Equation 7 is spatially discretized using second-order accurate central differences, and a consistent integration scheme is used to evaluate $\hat{N}$. The details of this formulation can be found in.[1,15,16,17]

Panel states are collocated into a single array $\mathbf{x}$ point-by-point,

$$\mathbf{x} = [v_1, w_1, v_2, w_2, ..., v_{N_x}, w_{N_x}],$$

leading to a state vector of dimension $2N_x$. In a similar fashion, an array $\mathbf{f}$ is defined to yield the spatially discrete system of equations $\frac{dx}{dt} = f(\mathbf{x}, \lambda)$, where the pressure parameter λ is selected to be a free variable.

$N_x = 31$ is chosen as the baseline mesh with 36 time intervals per cycle. High speed flow at $M_\infty = 10$ and mass-ratio, $\mu = 0.1$ is considered. The constraint equations are defined by the parameters β_1 and β_2, which are chosen to be a specified panel deflection (β_2) at a vanishing value of panel velocity (β_1), at the first grid point of the panel. Deflections are normalized by panel thickness, $h = 0.001$. The free variable λ in this problem is the nondimensional dynamic pressure.

Due to the presence of a larger number of variables compared to the airfoil problem, the construction of good initial conditions for the panel problem is far less straightforward. For a selected value of λ, time integration is carried out and the data ($\mathbf{X}$) is used to serve as initial condition. This point on the bifurcation curve is selected to correspond to $\beta_2 = -9 * 10^{-6} (\lambda = 4288)$. Using this data as initial condition, the entire bifurcation curve is generated by slowly incrementing β_2, and using the previous solutions as initial approximations in each calculation. This procedure has been carried out with the three different methodologies with the 36 degrees of freedom and is shown in Figure 8. A similar study was done[1] comparing the Cyclic/FD solution with Dowell's[15] 6-mode Galerkin representation of the panel equations. It was also shown that the baseline solution was well converged both in space and time. Note from Figure 8 that all three methodologies predict the curve perfectly, but for points on the strong nonlinear part of the curve, data points do not overplot. The high-order Time Spectral method and P-extension Spectral Element method are spot on but the second-order Finite Difference and h-extension Spectral Element digress a little.

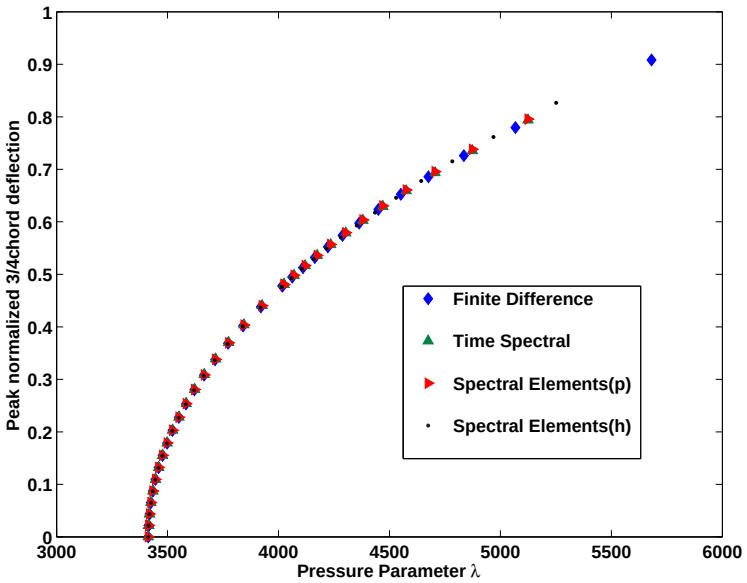

Figure 8. Peak LCO values of panel deflection at 3/4 chord position at different values of λ beyond the Hopf bifurcation point : Prediction of the bifurcation curve using different methods

IV. Conclusions and Future Work

Two spectral based computational techniques were implemented in combination with the cyclic method for the numerical prediction of LCOs. The time spectral method based on global basis functions captured rapid-transients with few DOF, but could prove to be prohibitive for large systems with substantial harmonic content since it produces full matrices. The spectral element method was used in a novel way with the cylic

method for periodic systems in time. This method produces sparse matrices and uses high-order polynomials to ensure high accuracy. An adaptive Cyclic/Spectral Element method was used to refine h in regions of steep-transients where higher resolution might be required. This showed better than exponential convergence, thus demonstrating potential for hP convergence.

A simple aeroelastic model of an airfoil with nonlinear structural coupling was studied in detail. Also a more challenging problem, a 2D nonlinear panel in high speed flow was studied using the new techniques.

For the future, we want to improve the efficiency of the numerical formulations, especially the iterative process which currently takes up most of the CPU time. Right now, the three methods use the full matrix formulation only dependent on the dimensionality of the problem. Ideally, we want to take advantage of the structure of the Jacobian matrix for the Newton iteration in each of the methods to estimate the true computational time. This way we can compare the relative merits of the methods.

In this paper, we have manually refined the time intervals for the adaptive Cyclic/Spectral element formulation. In the future, we would like to automate this process by taking account of the gradients and also the distribution of nodal points in each interval.

V. Acknowledgement

The authors would like to thank the Air Force Office of Scientific Research (Dr. Fariba Fahroo, PM) for the support of this work through LRIR 03VA01COR.

References

[1]P.S. Beran and D.J. Lucia. A reduced order cyclic method for computation of limit cycles. *Nonlinear Dynamics*, 39:143–158, 2005.

[2]A. Gopinath and A. Jameson. Time spectral method for periodic unsteady computations over two- and three-dimensional bodies. *AIAA paper 05-1220*, AIAA 43rd Aerospace Sciences Meeting and Exhibit, Reno, NV, January 10-13 2005.

[3]K.C. Hall, J.P. Thomas, and W.S. Clark. Computation of unsteady nonlinear flows in cascades using a harmonic balance technique. *AIAA Journal*, 40(5):879–886, May 2002.

[4]A.T. Patera. A spectral method for fluid dynamics: Laminar flow in a channel expansion. *J. Computational Physics*, (*54:468*), 1984.

[5]G.E. Karniadakis and S.J. Sherwin. *Spectral/hp Element Methods for CFD*. Oxford University Press, 1999.

[6]D.Lee and D.H.Hodges. A multi-flexible-body aeroelastic analysis of rotating systems with flexible components. *AIAA paper 02-1603*, 43rd AIAA/ASME/ASCE/AHS/ASC Structures, Structural Dynamics and Materials Conference, Denver, Colorado, April 22-25 2002.

[7]M.Borri. Helicopter rotor dynamics by finite element time approximation. *Computers and Mathematics with Applications*, Vol. 12A, No.1:149–160, January 1986.

[8]M. McMullen, A. Jameson, and J.J. Alonso. Acceleration of convergence to a periodic steady state in turbomachinery flows. *AIAA paper 01-0152*, AIAA 39th Aerospace Sciences Meeting, Reno, NV, January 2001.

[9]M. McMullen, A. Jameson, and J.J. Alonso. Application of a non-linear frequency domain solver to the euler and navier-stokes equations. *AIAA paper 02-0120*, AIAA 40th Aerospace Sciences Meeting and Exhibit, Reno, NV, January 2002.

[10]A. Quarteroni C. Canuto, M.Y. Hussaini and T.A. Zang. *Spectral Methods in Fluid Dynamics; Springer Series in Computational Physics*. Springer Verlag, 1988.

[11]E. Van der Weide, A. Gopinath, and A. Jameson. Turbomachinery applications with the time spectral method. *AIAA paper 05-4905*, 17th AIAA Computational Fluid Dynamics Conference, Toronto, Ontario, June 6-9 2005.

[12]B. Lee, L. Jiang, and Y. Wong. Flutter of an airfoil with a cubic restoring force. *AIAA*, 1998-1725, April 1998.

[13]D.R. Millman, P.I. King, and P.S. Beran. A stochastic approach for predicting bifurcation of a pitch and plunge airfoil. *AIAA*, 2003-3515, June 2003.

[14]C.L. Pettit and P.S. Beran. Effects of parametric uncertainty on airfoil limit-cycle oscillation. *Journal of Aircraft*, 40(5):1004–1006, Sep-Oct 2003.

[15]E.H. Dowell. Nonlinear oscillations of a fluttering plate. *AIAA Journal*, 4(7):1267–1275, July 1996.

[16]P.S.Beran, D.J.Lucia, and C.L.Pettit. Reduced order modelling if limit-cycle oscillation for aeroelastic systems. *ASME 2002-32954*, Proceedings of IMECE '02, New Orleans, LA, November 2002.

[17]R.P.Selvam and S.A.Morton. Computation of nonlinear viscous panel flutter using a fully implicit aeroelastic solver. (*98-1844*), 1998.